Dynamic Behavior Analysis of a Three-Phase BLDC Motor under Scalar Control Strategy for Automotive Actuation Systems

Ciprian Bejenar
Faculty of Electrical Engineering and Computer Science
University "Ştefan cel Mare" of Suceava
Suceava, Romania
bejenar.ciprian@gmail.com

Nicolae Daniel Irimia, Marian Luchian, Florin Ioan Lazar
Autonomous, Mobility and Safety (AMS) Department
Continental Automotive Romania SRL
Iasi, Romania
{daniel.irimia, marian.luchian, florin.lazar}
@continental-corporation.com

***Abstract*—As the automotive industry is increasingly focusing on development of both partially and full-electric vehicles, the improvement and further concepts analysis of electric drive systems represents a priority for adopting the best cost-performance solutions. This paper proposes a theoretical study followed by a simulation analysis of the dynamic response of an electrical actuator system driven by scalar control algorithm that can provide corresponding drive signals to (either) a Permanent Magnet Synchronous Motor (PMSM) or a Brushless Direct Current (BLDC) motor. For the basic design of the PMSM / BLDC motor was intensively used the Finite Element Method (FEM) software tool to obtain a more realistic and plausible model. The equivalent mathematical model of the proposed system (and its basic components) was further implemented in MATLAB / Simulink software environment for extended analysis under both static and dynamic operating conditions. One of the basics objectives of this study is to analyze the possibility of further integration of this type of systems into electric vehicles platforms, such as brake-by-wire or steering actuation systems.**

Keywords—scalar control; PMSM; BLDC; behavior analysis; actuation system; brake-by-wire; motor drives.

I. INTRODUCTION

The *Permanent Magnet Synchronous Motor (PMSM)* is a combination between an AC induction motor and a DC brushless motor. It has sinusoidal distributed stator windings and permanent magnets in its rotor structure. In parallel, the *Brushless Direct Current (BLDC)* motor usually has a similar rotor structure as that of a PMSM, but with the basic difference that the stator is comprised of apparent poles instead of distributed windings. The power density of (either) PMSM / BLDC motors is higher than that of AC induction motors when comparing the same ratings and necessary volume material. The rare-earth permanent magnets from the rotor structure provide a high-density magnetic field without external power consumption [1][2].

Today, these motors are designed to be more powerful by providing a higher torque-to-current ratio, a higher torque-to-volume ratio, a lower mass and a lower moment of inertia, which translates into higher efficiency and thus higher output power density. Because of their performance characteristics, these types of motors have applicability in the automotive domain, which includes pumps, compressors, blowers and servo-drives, while being also suitable for electric vehicles and dynamic energy recuperation systems which includes technologies like regenerative braking (Fig. 1).

Fig. 1. A Brushless Permanent Magnet Motor (BPMM) – specifically a BLDC motor used as the main actuator in innovative brake systems [3].

Usually, the synchronous motors must be driven aided by an electronic controller, commonly called *Variable Frequency Drive (VFD)* [4]. Specifically, BLDC motors can be driven under a trapezoidal control strategy, but also under a sinusoidal control strategy like scalar control (therefore the PMSM / BLDC motor analogy) [5].

II. MATHEMATICAL MODEL OF THE THREE-PHASES PMSM / BLDC MOTOR

A. Stator Phases Voltages Equations

The generic matrix form representation of the stator phases voltages equations corresponding to the 3-phases PMSM / BLDC motor can be expressed in static *(a,b,c)* frame of reference, as (extended form, that includes useful and leakage, self- and mutual-inductance components, saturation / variation

978-1-7281-6870-8/20/$31.00 ©2020 IEEE

depending on currents and mechanical rotor position) as in [6], [7], [8] and [9]:

$$\overbrace{\begin{bmatrix} u_A \\ u_B \\ u_C \end{bmatrix}}^{u_{ABC}(t)} = \overbrace{\begin{bmatrix} R_A & 0 & 0 \\ 0 & R_B & 0 \\ 0 & 0 & R_C \end{bmatrix}}^{R_{ABC}(temp)} \cdot \overbrace{\begin{bmatrix} i_A \\ i_B \\ i_C \end{bmatrix}}^{i_{ABC}(t)} + \frac{d}{dt} \cdot \overbrace{\overbrace{\begin{bmatrix} \overbrace{(L_{uA}+L_{lA})}^{L_A} & M_{AB} & M_{AC} \\ M_{BA} & \overbrace{(L_{uB}+L_{lB})}^{L_B} & M_{BC} \\ M_{CA} & M_{CB} & \overbrace{(L_{uC}+L_{lC})}^{L_C} \end{bmatrix}}^{L_{ABC}(t)=L_{ABC}(i_{ABC},\theta_e)} \cdot \begin{bmatrix} i_A \\ i_B \\ i_C \end{bmatrix}}^{\Psi_{sABC}(t)=L_{ABC}(t)\cdot i_{ABC}(t)= =L_j(t)\cdot i_j(t)+\sum_{\substack{j=A \\ j'=B \\ j\neq j'}}^{C} M_{jj'}(t)\cdot i_{j'}(t)} - \ldots$$

$$\ldots - \omega_e \cdot \Psi_{PM} \cdot \overbrace{\begin{bmatrix} sin(\theta_e) \\ sin\left(\theta_e - \frac{2\cdot\pi}{3}\right) \\ sin\left(\theta_e + \frac{2\cdot\pi}{3}\right) \end{bmatrix}}^{k_{\theta_e}} \quad \overbrace{\frac{d\Psi_{rABC}}{dt} = \frac{d\Psi_{PM-ABC}}{dt} = \overbrace{e_{ABC}(t)}^{e_{ABC}(\theta_e,\omega_e)}}$$

(1)

where:

t = continuous time [Hz^{-1}] or [s];

j = stator phase index, with $j \in \{A, B, C\}$ [-];

$u_{ABC}(t)$ = (column) matrix form representation of stator phase instantaneous voltages [Wb/s] or [V];

$i_{ABC}(t)$ = (column) matrix type representation of stator phase instantaneous currents [C/s] or [A];

$R_{ABC}(temp)$ = (square) matrix of self-electric instantaneous resistances of stator phase windings dependent on temperature "*temp*" [S^{-1}] or [Ω];

temp = temperature of each considered element [°C];

$\psi_{sABC}(t)$ = (square) matrix of (linkage and leakage) stator instantaneous magnetic flux components produced by self- and mutual inductances and currents flowing through each stator phase "j" winding [V·s] or [Wb];

$L_{ABC}(t) = L_{ABC}(i_j,\theta_e)$ = (square) matrix of self- and mutual stator phase instantaneous inductances depending on stator phase currents and electrical angular position [H];

$L_{uj}(t)$ = useful instantaneous inductance component of stator phase "j" [H];

$L_{lj}(t)$ = leakage instantaneous inductance component of stator phase j [H];

$\psi_{PM\text{-}ABC}(t)$ = (column) matrix of instantaneous magnetic flux (linkage) components of rotor PMs which traverses air gap and ferromagnetic stator core of each phase "j" [V·s] or [Wb];

$\Psi_{PM}(temp)$ = maximum value / amplitude of magnetic flux (linkage component) of rotor's PMs which traverses air gap and ferromagnetic stator core (temperature dependent) [V·s] or [Wb];

$e_{PM\text{-}j}(\theta_e, \omega_e) = e_j(\theta_e, \omega_e)$ = (column) matrix of resulting instantaneous back-electromotive forces (BEMFs) of each stator phase winding dependent on PM rotor flux variation with electrical angular velocity and position [Wb/s] or [V];

$\omega_e(t) = 2\cdot\pi\cdot f_e = d\theta_e/dt$ = electrical angular velocity (pulsation) [rad·Hz] or [rad/s];

f_e = electrical frequency [s^{-1}] or [Hz];

θ_e = electrical angular position [rad].

B. Electromagnetic Torque Equation

The total electromagnetic torque developed by the 3-phases PMSM / BLDC motor can be represented in static *(a,b,c)* frame of reference, as in [6], [7], [8] and [9]:

$$T_e(t) = \sum_{j=A}^{C} T_{ej}(t) = \sum_{j=A}^{C} \frac{e_j(t)\cdot i_j(t)}{\omega_m(t)} \Leftrightarrow$$

$$\Leftrightarrow T_e(t) = \frac{e_A(t)\cdot i_A(t) + e_B(t)\cdot i_B(t) + e_C(t)\cdot i_C(t)}{\omega_m(t)} \Leftrightarrow$$

$$\Leftrightarrow T_e(t) = -p\cdot\Psi_{PM}\cdot\begin{bmatrix} sin(\theta_e)\cdot i_A(t) + \ldots \\ \ldots + sin\left(\theta_e - \frac{2\cdot\pi}{3}\right)\cdot i_B(t) + \ldots \\ \ldots + sin\left(\theta_e + \frac{2\cdot\pi}{3}\right)\cdot i_C(t) \end{bmatrix}$$

(2)

where:

$\omega_m(t) = 2\cdot\pi\cdot f_m = d\theta_m/dt$ = mechanical angular velocity [rad·Hz] or [rad/s];

f_m = mechanical frequency [s^{-1}], [Hz] or [rot/s];

θ_m = mechanical angular position (of rotor) [rad];

p = number of rotor pole pairs (PMs) [-].

C. Movement Equation (Equilibrium of Torques)

The movement equation, also known as equilibrium of torques, can be expressed in a generic form as in [6], [7], [8] and [9]:

$$\overbrace{T_e(t)}^{\text{Electromagnetic Torque}} = \overbrace{J\cdot\frac{d\omega_m(t)}{dt}}^{\text{Inertial Torque, } T_J(t)} + \overbrace{\overbrace{\beta\cdot\omega_m(t)}^{\text{Viscous Friction Torque, } T_{fv}(t)} + sign[\omega_m(t)]\cdot \overbrace{T_C(t)}^{\text{Coulomb Friction Torque}}}^{\text{Friction Torque, } T_f(t)} + \overbrace{T_L(t)}^{\text{Load Torque}}$$

(3)

where:

$T_e(t)$ = total instantaneous electromagnetic torque developed by the motor [kg⋅m²/s²] or [N⋅m];

J = rotor's (and other's synchronously rotating elements connected to it) moment of inertia [kg⋅m²];

β = viscous friction coefficient [kg⋅m²/(rad⋅s)] or [N⋅m/(rad/s)];

$sign[\omega_m(t)]$ = sign of mechanical angular velocity of rotor, with $sign[\omega_m(t)] \in \{-1;0;1\}$ [-];

$T_C(t)$ = Coulomb friction torque [kg⋅m²/s²] or [N⋅m];

$T_L(t)$ = load torque [kg⋅m²/s²] or [N⋅m].

III. Scalar Control Algorithm

A. Technical Background Overview

The *Scalar Control* (also known as *V/Hz Control*) regulates only the magnitude and the frequency (~ electrical speed) of the related components, such as voltages, currents and resulting rotating magnetic field corresponding to the stator phases in such a way that the resulting flux is maintained at the desired (ideally constant) value during steady-state regime (4) [10]. By knowing the basic speed equation of synchronous motors (5) and its correlation with the supply voltage frequency (6), these must be set according to the desired speed of the resulting rotating magnetic field [11][12][13].

$$k = U / f \tag{4}$$

$$n = 60 \cdot f / p \tag{5}$$

$$f = n \cdot p / 60 \tag{6}$$

Thus, the supply voltage is proportionally adjusted to keep a constant ratio between voltage and frequency as it can be seen in Fig. 2 and to further maintain the magnetic flux in the motor air gap region at relatively constant values. Basically, only the rated minimum and maximum frequency information is needed to implement this profile [10].

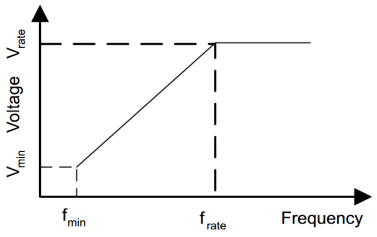

Fig. 2. Generic profile of the U/f characteristic used in scalar control [10].

One of the basic limitations of the scalar control algorithm is that the instantaneous angle between the resultant magnetic flux vectors corresponding to stator and rotor cannot be directly controlled (thus the internal angle of the motor is self-regulated naturally depending primarily on the mechanical load present at the rotor shaft). This qualifies the scalar control as one of the simplest algorithms that can be used for driving a PMSM / BLDC motor in correlation with a VFD [4]. For a more precise control other algorithms can be also considered, such as *Field-Oriented Control (FOC)* for example, that provides a better accuracy and performance, but with the cost of higher complexity and higher computational power required for its implementation [14].

B. Open-Loop Scalar Control Topology

The proposed paper treats the open-loop scalar control algorithm implementation topic without any feedback from the motor (e.g. speed, position or torque signals). This makes the algorithm quite easy to implement (due to its simplicity), with low demands in terms of computation power of the control hardware, but also with some additional disadvantages. One of these drawbacks is the instability of the system at certain frequencies [4].

Synchronous motors have their intrinsic property that the rotor strictly follows the rotating magnetic field (under certain limits and for specific working conditions). In case of open-loop scalar control topology the resultant magnetic field vector can rotate at different velocities that are proportional to (corelated with) the frequency of the power supply voltage(s). As long as the synchronism between stator and rotor magnetic fluxes is maintained, the only "error" that occurs is the self-adjusted internal angle (naturally regulated, basically depending on the load torque present at the rotor shaft). This represents the electrical angle between the resultant magnetic flux vectors of stator (energized coils) and rotor (permanent magnets) respectively [11][12].

IV. Finite Element Analysis (FEA) and Design of the Three-Phases BLDC Motor

To obtain a realistic and plausible BLDC motor model, the Finite Element Method / Analysis (FEM / FEA) simulation environment was used as the basic preliminary design tool. The motor model presents a symmetrical structure, provided with 12 stator slots and 10 rotor poles (permanent magnets – PMs).

The stator phase windings are arranged in a concentrated manner, as it can be seen in Fig. 3. The concentrated winding layout offers the advantage of increased pole pair numbers for reduced external diameters of the stator. Also, fractional number of slots per pole configurations can be designed with different performances. As the windings are closer to each other, the end windings are reduced, contributing to a shorter over-all length of the machine design. A drawback of this winding layout is that the harmonic content will be slightly higher compared to regular winding topologies.

The stator and rotor ferromagnetic cores are made up of standard iron-silicon (*FeSi*) material disposed in lamination sheets insulated from each other to reduce the Hysteresis and Eddy current losses.

The permanent magnets from the rotor structure are made up of rare-earth Neodymium Iron Boron (*NdFeB*) material and are disposed at its surface (outer periphery) to reduce the reluctance variation with respect to angular position. Notches are required on the rotor surface, in the case of surface

permanent magnets, in order to reduce the flux leakage between adjacent magnets.

The geometric design and the resulting saturation of the ferromagnetic cores (determined by the magnetic flux density / magnetic induction) of the BLDC motor at 1000 rpm in normal mode operation (nominal sine-wave currents – imposed) can be seen in the same figure, where the dark blue signifies a very low magnetic induction of about ~10^{-6} T and the light yellow signifies a high magnetic induction of about ~2 T as in [6], [7], [8] and [9]. The saturation of ferromagnetic circuit is determined by the strength of the resulting magnetic field produced by the active / energized stator phases and the rotor permanent magnets (thus being dependent by both rotor position and phase currents amplitudes). As can be observed, the design may implement some geometrical optimization to avoid stator saturation in the teeth end area. Furthermore, the average saturation of both yokes is reduced, which could lead in higher loading capability of the motor with an optimized design.

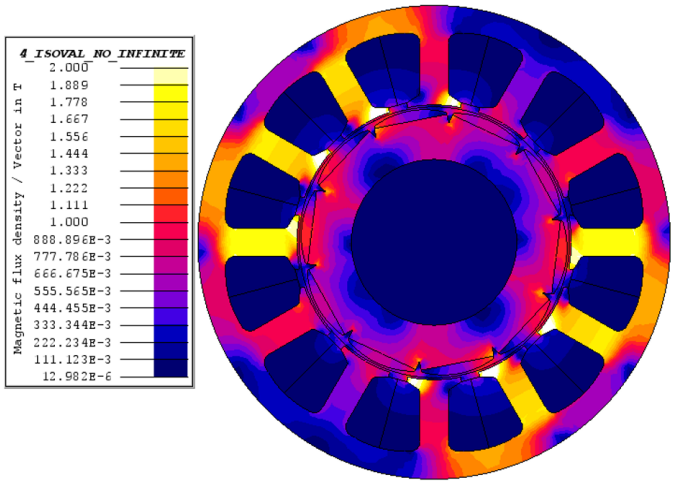

Fig. 3. FEA 3-phases BLDC motor concept overview provided with 12 stator slots and 10 rotor poles [8], [9], [10] and [11].

Each stator phase self-inductance component of the BLDC motor has a non-linear dependency of both current (because of saturation of ferromagnetic core) and mechanical angular position of rotor respectively (variable reluctance).

Consequently, by using a FEM / FEA tool, a close to reality equivalent BLDC motor model was developed, with basic parameters that were further transferred in MATLAB / Simulink environment for extensive analysis of its behavior under scalar control regime and for different dynamic working conditions.

V. MATLAB / SIMULINK MODEL OVERVIEW

A brief overview of the scalar control drive system is presented in a diagram, as shown in Fig. 4.

Fig. 4. General diagram of the scalar control based proposed drive system.

The proposed control algorithm provides three-phases (ideally) sinusoidal power supply voltages that are further used to drive the equivalent mathematical model of PMSM / BLDC motor. The amplitude and frequency of the supplied sine waves varies according to the imposed U/f characteristic, respectively synchronous to the requested mechanical rotor speed (or the equivalently derived mechanical rotor position) multiplied with the number of pole pairs.

Operation mode, as explained on the basis of the general diagram, can be easily observed on the simulated system. Functional key elements are also explained referring to Fig. 6 and Fig. 7 (and associated descriptions) to understand the outputs of each structural element, but also to Fig. 8 - 16 (and associated descriptions), to understand how the final element outputs are responsively varying depending on the supplied inputs.

The MATLAB / Simulink software environment was further used to implement the mathematically equivalent model (described with basic equations) of the PMSM / BLDC motor and the corelated designed open-loop scalar control algorithm (Fig. 5).

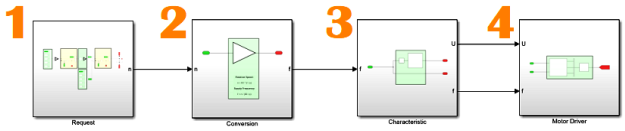

Fig. 5. MATLAB / Simulink scalar control algorithm architecture – model overview.

Each basic components (subsystems) of the proposed open-loop scalar control model are further detailed explained.

- *Block 1* represents the user control / command panel. It allows the operator to select / request / provide either the mechanical rotor position or speed control reference. The position control allows to impose (request) either fixed or variable electrical position $\theta_e(t)$ *[°]* further transformed into equivalent mechanical position $\theta_m(t)$ *[°]* at the motor shaft (providing the possibility for positioning applications). The requested instantaneous mechanical position is converted (derived) into the equivalent mechanical rotor speed in time *n(t) [rpm]* by applying equation (7) [11][12].

$$n(t) = (d\theta_e(t) / dt) \cdot (\pi / 180) \cdot (60 / 2\pi) \quad (7)$$

  In case the speed control is selected, this block also allows the direct imposition of either fixed or variable mechanical rotor speed reference.

- *Block 2* includes a conversion block that transforms the requested instantaneous mechanical rotor speed *n(t)* from *[rpm]* (by classically division to *60 [s]* and further multiplication with the number of rotor's pole pairs *p [-]*) to the equivalent instantaneous electrical frequency $f_e(t) = f(t)$ *[Hz]*, as in equation (8) [11][12].

$$f(t) = n(t) \cdot p / 60 \quad (8)$$

- *Block 3* implements the basic algorithm that includes the specific U/f characteristic and further provides at its outputs the instantaneous three-phases (ideally) sinusoidal voltages *u(t) [Wb/s]* or *[V]* characterized by a certain frequency $[s^{-1}]$ or *[Hz]*.
- *Block 4* comprises the *Voltage Source Inverter (VSI)*. It generates three-phases sinusoidal supply voltages (by additionally taking into consideration some possible voltage drops and power losses of basic electrical components that usually can be found on the current path of a typical power inverter). In real (physical) systems, for an inverter connected at 13.8 V Direct Current (DC) power supply (e.g. a car battery), due to the semiconductor and converter losses, the output voltages may reach only 8.9 V or 12.6 V at peak as it can be seen in Fig. 6 and Fig. 7 respectively.

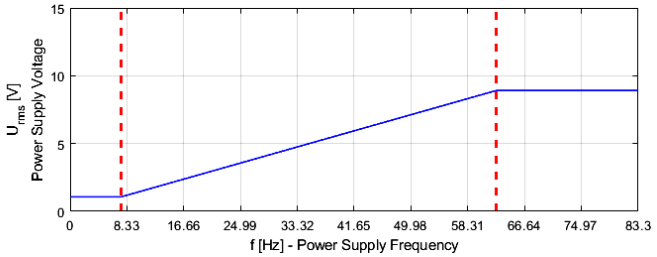

Fig. 6. The sine wave amplitude vs. frequency of voltage power supply obtained at the outputs of the *Voltage Source Inverter (VSI)* block, according to the imposed U/f characteristic.

Minimum supply voltages were chosen such as the resulting phase currents are kept below the maximum admissible value while the corelated resulting magnetic field strength (intensity) is also high enough to further develop the corresponding electromagnetic torque.

During the process of obtaining the instantaneous phase voltages corresponding to a symmetrical and balanced three-phase sinusoidal regime, it was necessary to firstly provide an equivalent three-axis (α,β,γ) stationary reference frame (implementing a simplified analogous version of Clarke transformation – available for both constant and variable electrical pulsation), described by equation (9) [15] [16].

$$\begin{cases} u_{\alpha}(t) = U_{rms}(t) \cdot \sqrt{2} \cdot \cos\left(2 \cdot \pi \cdot \int f(t)dt\right) \\ u_{\beta}(t) = U_{rms}(t) \cdot \sqrt{2} \cdot \sin\left(2 \cdot \pi \cdot \int f(t)dt\right) \\ u_{\gamma}(t) = 0 \end{cases} \quad (9)$$

where: $u_{\alpha}(t)$ and $u_{\beta}(t)$ are the voltage components corresponding to the symmetrical and balanced regime, while $u_{\gamma}(t)$ is the homopolar component (which is considered to be zero for this specific case) of the stationary reference frame.

Another required step is to convert $u_{\alpha,\beta,\gamma}(t)$ voltage components into $u_{A,B,C}(t)$ phase voltages by operating with inverse Clarke transformation [15] [16].

Increasing the requested mechanical rotor speed from 0 rpm to 1000 rpm during a time interval of 1 s, the VSI will synchronously generate adequate sine wave power supply voltages of specific frequencies ranging from 0 Hz to 83.33 Hz during the same time interval (Fig. 7). The resulting waveforms are desired to present an ideally sinusoidal shape.

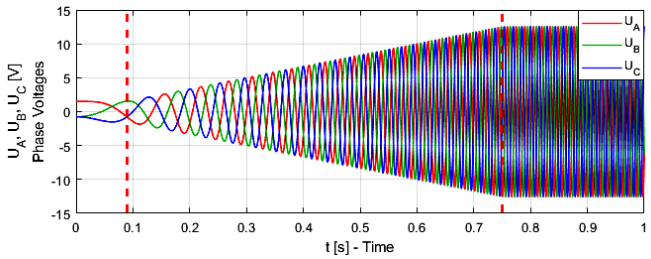

Fig. 7. Instantaneous phase voltages $u_A(t)$, $u_B(t)$ and $u_C(t)$ provided by the Voltage Source Inverter (VSI) according to the predefined U/f characteristic.

As for the mathematical model of the three-phases BLDC motor, it was developed by considering both the particularities of the previously obtained FEA design, combined with some simplified assumptions. Thus, the basic parameters of the BLDC motor model from FEM analysis are further transferred in MATLAB / Simulink software environment as an equivalent model. Both FEA design and equivalent mathematical model of BLDC motor imply some simplifying assumptions, such as in [8], [9], [10] and [11]:

- anisotropy of stator and rotor ferromagnetic circuits is omitted;
- stator phases are symmetrically distributed in slots;
- stator phase windings have the same number of turns;
- permanent magnets (PMs) from rotor structure are evenly arranged at its outer periphery.

As a further simplification, the simulation tests presented in this paper are done by neglecting the stator phase inductance saturation / variation with current and rotor position (here referring to MATLAB / Simulink environment).

VI. Simulation Results

By analyzing some preliminary simulations, it seems that the system inertia has a relatively high impact on the behavior (response) of the PMSM / BLDC motor under scalar control strategy.

The basic objectives of the next simulation tests are to determine both static and dynamic performances of the proposed PMSM / BLDC motor model when being driven by the open-loop scalar control algorithm and to eventually decide the possibility of further integration in brake-by-wire or steering actuation applications. It is also interesting to observe the impact of some specific motor parameters on the control system response. If the results are not as expected, a better design of the PMSM / BLDC motor is necessary to further compensate / diminish the necessity of using more complex and mathematically intensive control algorithms.

The mechanical (torque vs. speed) characteristic of the PMSM / BLDC motor is computed by slowly and progressively loading the motor at different operating speeds (by keeping it under steady-state conditions, thus running at synchronism). As shown in Fig. 8, by using scalar control strategy, the motor is capable to provide up to 10 N·m of mechanical torque. However, during dynamic operation conditions (where frequent accelerations and decelerations are expected), the motor is often running in quasi-permanent transient regimes and the resulting electromagnetic and further mechanical torque may not reach (or at least not constantly sustain) the mentioned peak values, therefore another request from the control algorithm is to compensate this effect correspondingly.

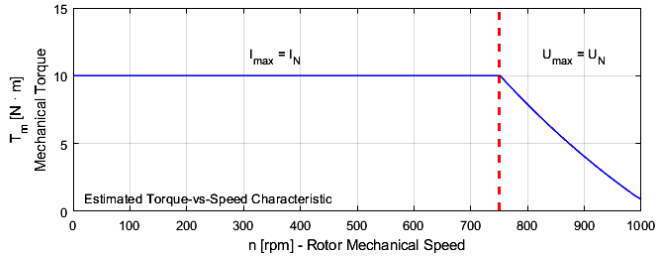

Fig. 8. Mechanical (torque vs. speed) characteristic of proposed BLDC motor model.

Depending on the test conditions, the scalar control algorithm provides and imposes a specific U/f profile (as seen in Fig. 6) that further determines corresponding (ideally) sine-wave phase voltages (as seen in Fig. 7) that further determine corelated sine-wave currents as shown in Fig. 9. The resulting currents were obtained by applying a constant load torque of 0 N·m at the rotor shaft.

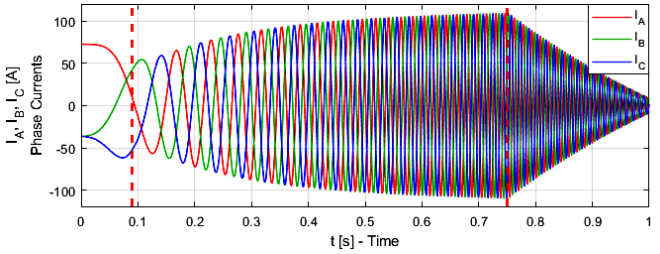

Fig. 9. Instantaneous phase currents $i_A(t)$, $i_B(t)$ and $i_C(t)$ corresponding to a load torque of 0 N·m.

The current vs. frequency dependency curve can be observed in Fig. 10. By using this simple control strategy, it seems that the system response is acceptable (within some error limits). Still, there is room left for possible improvements and optimization.

As it can be observed, the current profile is only partially maintained constant (and only within certain regions it achieves 100 % of its nominal / target value), therefore the capabilities of the motor in terms of electromagnetic and mechanical torque development may suffer some drops of almost 50 % at certain frequencies and speeds. This may lead to system instabilities that are related to the way the control algorithm performs.

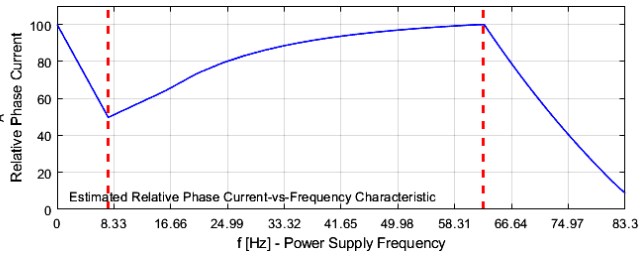

Fig. 10. Relative (trace / peak of) current vs. frequency characteristic.

Even if the presented scalar control algorithm is not yet fully optimized and can be further improved, it currently provides an interesting overview on the possible system response and performance when using a roughly simple control strategy in combination with a PMSM / BLDC motor. These preliminary results can be further used as a basis for further steps of research and development on related topics.

The dynamic behavior of this system is further highlighted by applying a mechanical load torque of 5 N·m at the rotor shaft of the PMSM / BLDC motor and by considering specific test conditions, such as:

A. Step-Response Analysis (Fig. 11 and Fig. 12);

B. Ramp-Response Analysis (Fig. 14 and Fig. 15);

C. Position Control Analysis (Fig. 16).

A. Step-Response Analysis

In this section is analyzed the behavior of the system when applying a step request from 0 rpm to nominal speed.

Because of the already mentioned scalar control limitations (specifically referring to its inability to impose / maintain a constant internal angle between stator and rotor magnetic fluxes of PMSM / BLDC motor), when the rotor starts to move some high ripples occur in its speed response as it can be seen in Fig. 11. Even under these circumstances, it seems that the system stability is still being achieved after about 0.1 s.

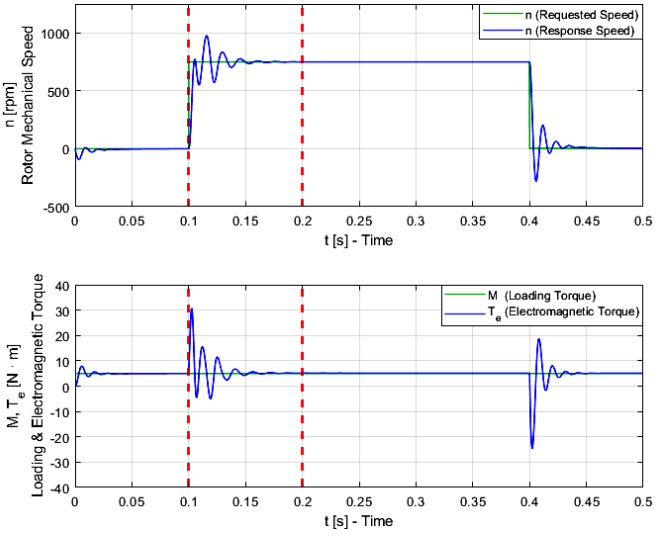

Fig. 11. Step-response of BLDC motor under scalar control.

By applying the Fast Fourier Transform (FFT), some high harmonics content can be observed in the current and electromagnetic torque waveforms as it can be seen in Fig. 12. This determines some undesired magneto-dynamic forces to manifest inside the motor structure that further determine specific vibrations that may over stress its electro-magnetic circuits.

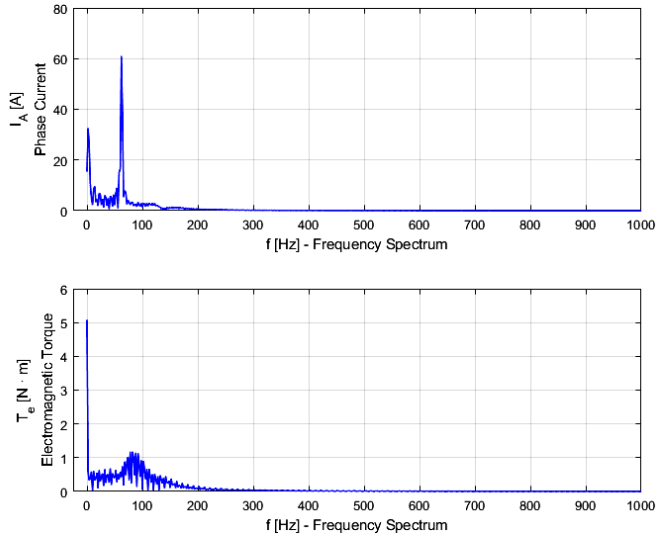

Fig. 12. FFT analysis for step-response of BLDC motor under scalar control.

B. *Ramp-Response Analysis*

To further optimize this system behavior, a simple approach was to diminish / eliminate sudden variations of the speed request (provided by the motor control algorithm). This was done by applying a custom parameterized low-pass filter (modeled by using equivalent transfer functions), shown in Fig. 13, in correlation with low rising slope ramp signals, as presented in Fig. 14.

By comparing the step-response against the ramp-response, it can be seen a great improvement in the dynamic behavior of the system in the second case. There are no longer present significant instabilities in the system response such as high ripples or spikes, so the PMSM / BLDC motor is running smoother. Additionally, the magnetic coupling between the permanent magnets from the rotor and the resulting rotating magnetic field produced by the stator active windings is more stable in this case, thus resulting lower variations of internal angle of the motor.

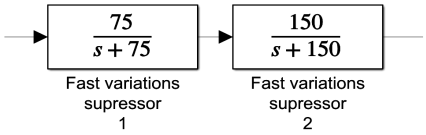

Fig. 13. Equivalent low-pass filter (comprised of series connected transfer functions) used to suppress fast variations of speed request.

When looking at the FFT results presented in Fig. 15, it seems that the harmonics content of absorbed current is greatly reduced compared to the previous case (specifically the ramp response). A smoother start-up with especially lower current peaks improves the lifecycle of the motor and also of the related equipment involved (due to less mechanical stress and resulting vibrations).

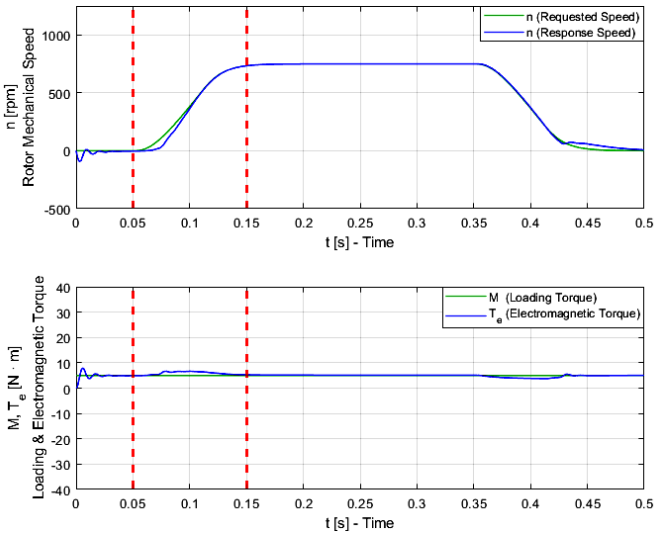

Fig. 14. Ramp-response of BLDC motor under scalar control.

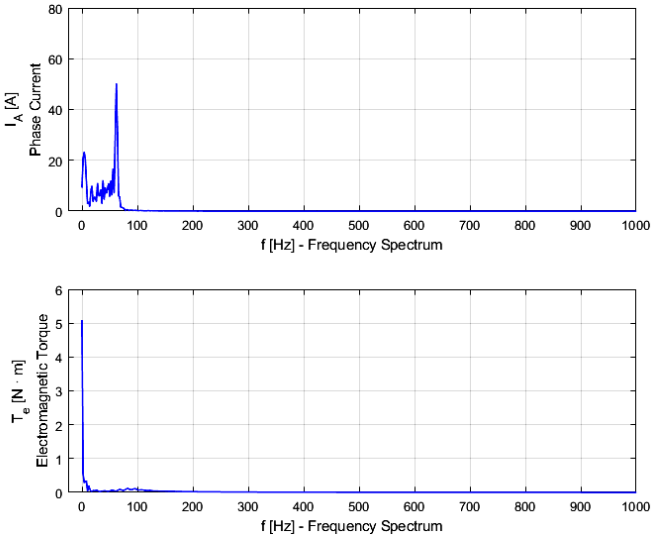

Fig. 15. FFT analysis for ramp-response of BLDC motor under scalar control.

C. *Position Control Behavior Analysis*

In this section was further analyzed the system response when applying position control mode (Fig. 16).

To avoid high ripples and possible system instabilities during the open-loop position control mode, the maximum variation of the requested position must not exceed $d\theta_e(t) / dt =$ 4500 °/s for this specific system parameterization. This limitation is due the risk of driving the motor into an instable regime that, depending on the loading torque, may cause the synchronism to break.

When requesting position variations greater than this specified value, through derivation, the imposed equivalent mechanical rotor speed will exceed the nominal speed.

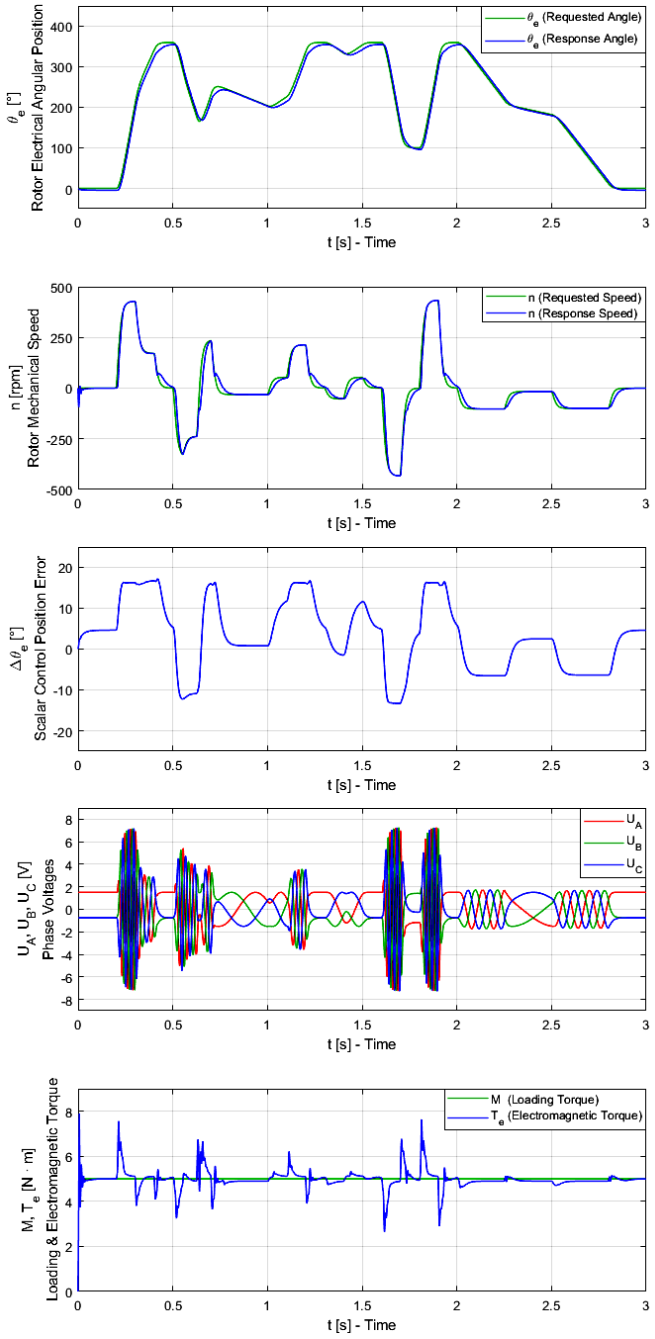

Fig. 16. Position control of BLDC motor under scalar control.

In contrast to the open-loop topology, in case of the close-loop strategy the resulting error (that is simply determined as the difference between the requested and the measured rotor position) is further used as input of the position regulators that provides adequate command signals to diminish / eliminate it.

As shown in Fig. 16, during the open-loop position control mode, this error is influenced by the rotor speed in conditions of a constant loading torque. An explanation is that at certain speeds there are system instabilities that occur. This has been previously encountered and analyzed in simulations and is a result due the lack of constant current over those periods.

VII. CONCLUSIONS

This paper presents the mathematically approach and further MATLAB / Simulink model implementation of an open-loop scalar control algorithm used to drive a specifically developed BLDC motor (modelled by using the FEA tool).

Although the motor design has a relatively high impact on the behavior of the actuation systems, of even higher importance is the control algorithm used for driving it.

The open-loop scalar control topologies are not among the most performant (or efficient) methods, but they still provide some advantages as simplicity and ease of implementation specifically for systems that do not require high-performance or high-precision results. Although the scalar control strategy is more widely used for driving AC induction motors, when applying it to synchronous motors, better performance is obtained due to the absence of the rotor slip phenomenon.

A further improvement of the proposed open-loop scalar control algorithm may consist in development and implementation of a more optimized U/f profile that can further compensate some of the basic disadvantages of the currently used profile.

Another step would be to develop a closed-loop control algorithm and to further analyze its behavior under similar test conditions (for comparison reasons) and its possibility of further integration in brake-by-wire or steering actuation systems from automotive domain.

REFERENCES

[1] https://www.infineon.com/cms/en/applications/solutions/motor-control-and-drives/permanent-magnet-synchronous-motor/

[2] G. Rata, M. Rata, I. Graur and D. L. Milici, “Induction motor speed estimator using rotor slot harmonics”, in Advances in Electrical and Computer Engineering (AECE), vol. 9, no. 1, pp. 70-73, 2009.

[3] https://www.motioncontrolonline.org/blog-article.cfm/Brushed-DC-Motors-Vs-Brushless-DC-Motors/24/

[4] Y. Parmar, P. Patel, N. Pancholi, C. Thakor and U. Mali, “Scalar control of permanent magnet synchronous motor”, in International Research Journal of Engineering and Technology (IRJET), vol. 3, no. 12, pp. 364-366, 2016.

[5] A. Rahim, N. Hassan and M. Muhammad, “Efficiency comparison of trapezoidal and sinusoidal method for brushless DC motor drive”, in Applied Mechanics and Materials, vol. 785, pp. 248-252, 2015.

[6] N. D. Irimia and F. I. Lazar, “A comparative study of different BLDC motor construction types used in automotive industry under specific command strategies”, 22nd IMEKO TC4 Symposium and 20th International Workshop on ADC Modelling and Testing, Iasi, Romania, 2017.

[7] N. D. Irimia, F. I. Lazar, M. Luchian and A. Ipatiov, “Improved fault tolerant control of a redundant actuation system provided with dual stator six phases BLDC motor for autonomous driving applications”, 22nd International Conference on System Theory, Control and Computing (ICSTCC), Sinaia, Romania, 2018.

[8] N. D. Irimia, F. I. Lazar and M. Luchian, “Comparison between sinusoidal and space vector modulation techniques on the resulting electromagnetic torque ripple produced by a three-phase BLDC motor under field-oriented control”, 6th International Conference on Control, Decision and Information Technologies (CoDIT), Paris, France, 2019.

[9] N. D. Irimia, F. I. Lazar and M. Luchian, “Robust fault tolerant control by using space vector modulation (SVM) technique of a five phases BLDC motor for autonomous driving applications”, in course of

publishing at – 7th International Conference on Control, Decision and Information Technologies (CoDIT), Prague, Czech Republic, 2020.

[10] B. Akin and N. Garg, "Scalar (V/f) control of 3-phase induction motors", in *Application Report (SPRABQ8),* Texas Instruments, 2013.

[11] R. K. Rajput, "A text book of electrical machines", Laxmi Publications, New Delhi, India, 2006.

[12] C. Busca, "Open loop low speed control for PMSM in high dynamic applications", Aalborg University, Denmark, 2010.

[13] G. Rata, C. Bejenar and M. Rata, "A solution for studying the DC motor control using NI MyRIO-1900", 8th International Conference on Modern Power Systems (MPS), Cluj-Napoca, Romania, 2019.

[14] M. Rata, G. Rata, L. D. Milici and I. Graur, "An efficient solution of the step-down converter for students teaching", in Elektronika ir Elektrotechnika, vol. 91, no. 3, pp. 77-80, 2009.

[15] B. K. Bose, "Power electronics and variable frequency drives: technology and applications", IEEE Press, 1997.

[16] M. Štulrajter, V. Hrabovcová and M. Franko "Permanent magnets synchronous motor control theory", in Journal of Electrical Engineering, vol. 58, no. 2, pp. 79-84, 2007.